



Experimental and simulation study of the ED-milling flow field to improve its machining performance

Chengbo Guo¹ · Shufa Sun¹ · Shichun Di² · Dongbo Wei²

Received: 21 October 2020 / Accepted: 8 February 2021 / Published online: 22 February 2021
© The Author(s), under exclusive licence to Springer-Verlag London Ltd. part of Springer Nature 2021

Abstract

In electrical discharge milling (ED-milling), the flow field of the working medium plays an important role in the removal of discharge eroded particles from the discharge gap. In this work, a flow field model between the electrode and workpiece was established based on analysis of the moving path of the eroded particles in the discharge gap. The influence of the single-layer cutting thickness and electrode diameter on the flow field and machining performance was studied via simulations and experiments. Three kinds of new structure electrodes containing multiple holes were designed to improve the eroded particle removal efficiency. The flow field and machining performance of ED-milling with these new electrodes were studied via simulations and experiments. Through the design of multiple holes surrounding the electrode outer wall, the flushing flow field was more conducive to the removal process of the eroded particles. By adopting the newly designed electrode, the ED-milling machining efficiency was improved by 33%.

Keywords ED-milling · Flow field · Electrode structure · Single-layer cutting thickness · Machining performance

1 Introduction

In sinking electrical discharge machining (EDM), the materials melted during the discharge process are ejected from the discharge area depending on the expansion and contraction movement characteristics of the gas bubble surrounding the discharge channel [1, 2]. The ejected melted materials are cooled and form eroded solid particles in the discharge gap, which are expelled from the discharge gap via intermittent electrode lifting movement. In wire EDM, eroded solid particles are removed from the discharge gap via movement of the wire and flow of the working medium [3, 4].

In ED-milling, discharge eroded solid particles are removed from the discharge gap mainly depending on the working medium flowing through the discharge gap [5–7]. The removal efficiency of the discharge eroded particles is

influenced by the flow velocity and volume of the working medium flowing through the discharge area. The flow volume influences the cooling effect and deionization effect of the discharge gap, while the flow velocity influences the efficiency of the removal of the eroded particles from the discharge gap. In ED-milling, the flow field of the working medium is the key to maintaining the stability of the machining process. An insufficient flow field could lead to an unstable discharge process, and the discharge eroded particles could readhere to the workpiece surface. As a result, effective material removal may not be realized. This could also result in instability of the subsequent discharge.

Considering the important role of the working medium in the eroded particle removal process, multiple working medium have been tested for ED-milling purposes [8]. Shen et al. [9] improved the maximum material removal rate of AISI 304 stainless steel to 5534 mm³/min by adopting arc discharge in ED-milling with high-speed air as the working medium. To address the difficulty of the removal of debris from the electrode bottom in EDM machining via high-aspect ratio small holes, Liu et al. [10] improved the machining performance by adopting side flushing under ultrasonic vibration assistance. Electrodes with new structures have been designed to improve the ED-milling machining performance [11]. Wang et al. [12] proposed a tool electrode with gas flushing inside the

✉ Chengbo Guo
chengbo.guo@nefu.edu.cn

¹ School of Engineering and Technology, Northeast Forestry University, Harbin, China

² School of Mechatronics Engineering, Harbin Institute of Technology, Harbin, China

electrode and liquid flushing outside the electrode to improve the machining performance of ED-milling, and their results showed that this working medium flushing method improved the debris expulsion capacity and discharge gap cooling performance. To realize better debris exclusion from the kerf in wire EDM, Okada et al. [13] investigated the flow field and debris movement in wire EDM-processed kerfs and found that based on the flow velocity variation over time, a reasonable flushing position and direction facilitated the debris exclusion process.

The simulation method has been adopted to study the ED-milling process [14–16]. Wang et al. [17] established a liquid-solid two-phase flow field model for inner-jetted dielectric ED-milling, and they observed that the material removal rate (MRR) and tool electrode wearing rate (TWR) were proportional to the dielectric inlet pressure. Shabgard et al. [18] studied the plasma channel flushing efficiency in the EDM process via simulation, and plasma flushing efficiency equations based on a regression model were established to predict the cardinal parameter of the recast layer thickness. Liao et al. [19] established a fluid dynamics model characterizing the motion of a square-shaped electrode, and their results indicated that the debris at the bottom could be removed more easily by adopting an electrode with a high jump speed.

It has been found that debris accumulation in the machining gap results in a low machining efficiency of the fast EDM hole drilling process at the hole breakthrough stage. Wang et al. [20] proposed a method of combined flushing involving a high-pressure tube-inner dielectric and high-velocity tube-outer dielectric configuration, which improved the machining efficiency at the breakthrough hole stage by 89%. To study the movement of bubbles and the location of discharge in the discharge gap, Kunieda et al. [21] adopted a transparent SiC single crystal as the tool electrode and observed the discharge process with a high-speed video camera. They found that radial flow and a certain bubble oscillation difference resulted in a higher material removal rate in water than that in oil owing to the viscosity of the working medium.

It is observed from the above research results that the flow field of the working medium plays an important role in the removal of eroded particles from the discharge gap between the electrode and workpiece. This research focuses on enhancing the ED-milling machining performance by improving the flow field of the working medium. Owing to the limited space of the discharge gap and the presence of a high-pressure flushing working medium, it is difficult to observe the flow field in the discharge gap. The flow field between the electrode and workpiece is studied based on simulations. The effect of the single-layer cutting thickness and electrode diameter on the machining performance is investigated. A new electrode structure is designed to optimize the flow field in the discharge gap based on the simulation results. A corresponding

experiment is designed to verify the eroded particle removal effect with the newly designed electrodes.

2 Establishment of the flow field model in ED-milling

2.1 Analysis of the flow field between the workpiece and electrode

In ED-milling, the desired product shape is realized with a tubular electrode to mill the workpiece in layers. The working medium flows into the discharge gap through the central hole of the tubular electrode to cool the discharge area and remove eroded particles. Rotation of the electrode uniformly wears the electrode edge and promotes the removal process of eroded particles from the discharge gap.

An illustration of ED-milling equipment and the flow field between the electrode and workpiece is shown in Fig. 1. As shown in Fig. 1a, the ED-milling equipment contains a machine body, computer numerical control (CNC) system, pulse power supply, and working medium flushing system. The feeding speed of the electrode is adjusted based on detection of the discharge status. A pressure gauge is connected to the inlet pipeline to measure the working medium flushing pressure. Owing to the influence of electrode wear during the discharge process, after a given period of ED-milling machining, the end of the electrode exhibits a uniform semicircular chamfer shape, as shown in Fig. 1b. Figure 1c shows a 3D model of the electrode and workpiece during the ED-milling process. Figure 1d shows the flow field distribution along the electrode feeding direction (the X direction). Electrical discharge mainly occurs in the front semicircular area along the electrode feeding direction, and most of the eroded particles are primarily generated in this area. The discharge eroded particles are largely washed away from the discharge gap along the electrode feeding direction. The working medium flowing along the direction opposite to the electrode feeding direction imposes a limited effect on the removal of discharge eroded particles from the discharge gap. Based on analysis of the cross-sectional flow field between the electrode and workpiece, it is observed that only the working medium flowing through the front semicircular area along the electrode feeding direction effectively removes eroded particles from the discharge gap.

2.2 3D model of the flow field

Considering the influence of electrode wear on the flow field, a three-dimensional flow field model was established, as shown in Fig. 2. The diameter of the central hole was 6 mm. The stable chamfer formed due to electrode wear was equal to

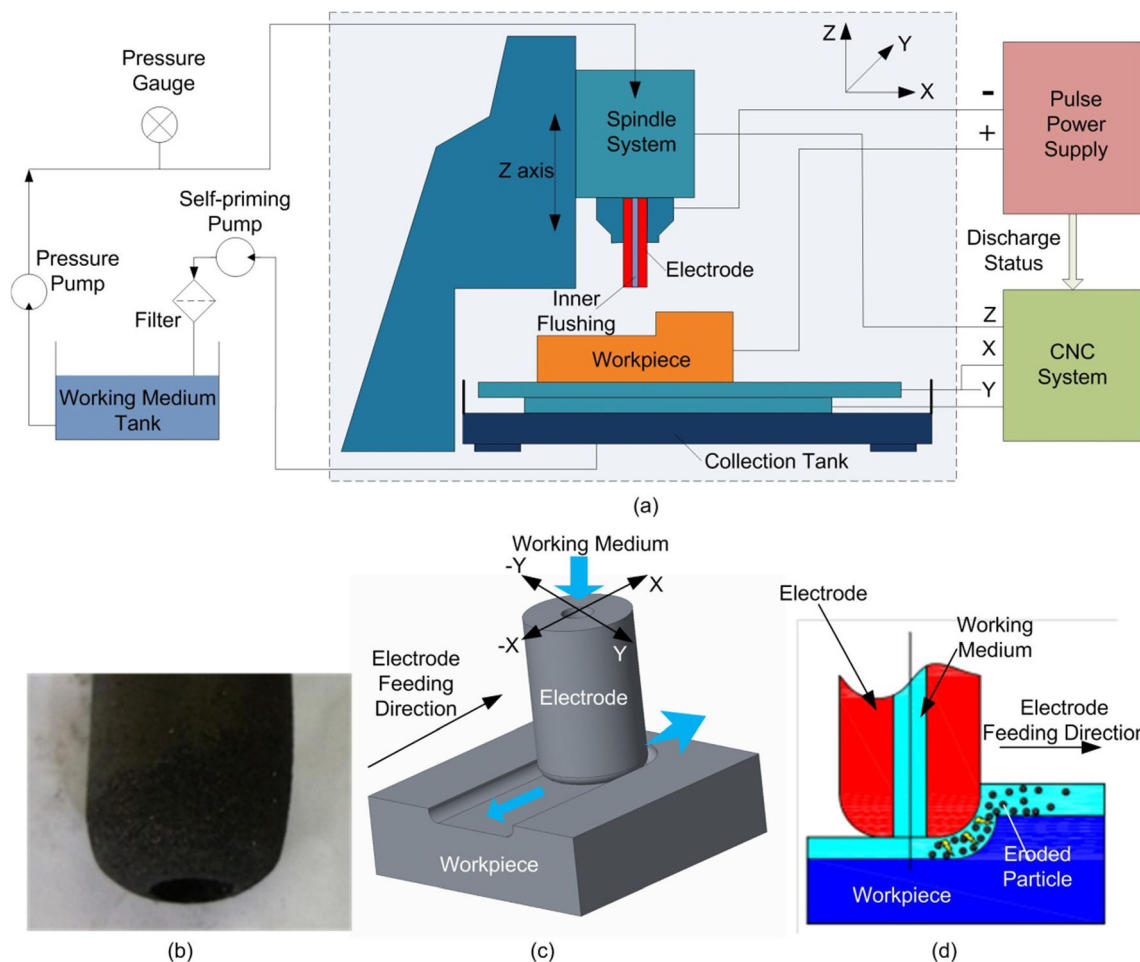


Fig. 1 The ED-milling process. **a** Schematic diagram of ED-milling equipment. **b** Shape of the electrode after wear. **c** Groove machining process via ED-milling. **d** Cross-sectional illustration of the ED-milling flow field

the single-layer cutting thickness. The discharge gap between the electrode and workpiece was 0.3 mm.

To facilitate analysis of the flushing effect, the working medium outlet is divided into 3 areas, as shown in Fig. 2. Since discharge primarily occurs in the front semicircular area where the electrode is the closest to the workpiece, only the working medium flowing from outlets 1 and 2 washes the

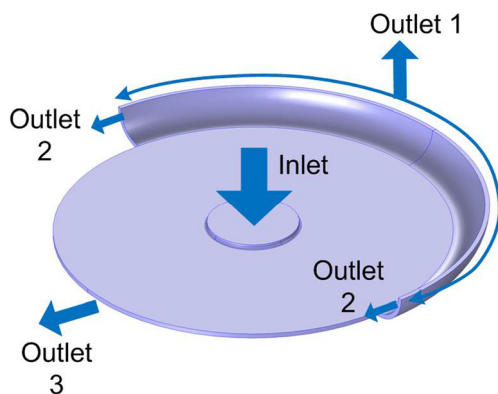


Fig. 2 3D model of the ED-milling flow field

discharge area and removes discharge eroded particles from the discharge gap, which is referred to as effective flushing in this research. The working medium flowing from outlet 3 is denoted as the auxiliary cooling working medium.

2.3 Mathematic model of the flow field

Fluid flow is divided into two states: laminar flow and turbulent flow. The flow state is influenced by the flow velocity, pipe diameter, dynamic viscosity, and fluid density. The Reynolds number (Eq. (1)) is adopted to determine the flow state of the working medium.

$$Re = \frac{\rho VL}{\mu} \tag{1}$$

where ρ is the density of the working medium, V is the working medium flow velocity, L is the characteristic length of the working medium flow pipe, and μ is the dynamic viscosity of the working medium.

In regard to pipe flow subject to a circular cross-section, the critical Reynolds number is 2000. The flow field is laminar

flow when the Reynolds number is smaller than 2000, and turbulent flow occurs when the Reynolds number is larger than 2000. The fluid used in ED-milling is a water-based working medium of a 5% emulsion in water. Its physical properties are similar to those of water. Therefore, the physical properties of water are adopted in flow field simulation. The characteristic length of the central inlet hole is 6 mm. In ED-milling, the pressure of the working medium at the inlet tube is 1.5 MPa at a flow velocity of 12 m/s. According to Eq. (1), the flow field in this research is turbulent flow.

Turbulent flow is characterized by a wide range of flow scales containing a certain number of interacting irregular vortices of various scales. The velocity and pressure at any point of the flow field in the flow process change overtime. The k - ε turbulence model is employed to analyze the flow field. The kinetic energy k and dissipation rate ε in the turbulent model are determined by its transmission equations.

The turbulence intensity is:

$$I = 0.16 \times (Re)^{-1/8} \quad (2)$$

The turbulent kinetic energy k is:

$$k = \frac{3}{2} \times (V \times I)^2 \quad (3)$$

The turbulent dissipation rate ε is:

$$\varepsilon = \frac{\mu^{0.75} \times k^{1.5}}{l} \quad (4)$$

The turbulent length scale is:

$$l = \frac{k^{3/2}}{\varepsilon} \quad (5)$$

The turbulent viscosity is modeled as:

$$\mu_T = \rho C_\mu \frac{k^2}{\varepsilon} \quad (6)$$

where C_μ is a model constant.

The transport equation for the turbulent kinetic energy is:

$$\rho \frac{\partial k}{\partial t} + \rho \mathbf{u} \cdot \nabla k = \nabla \cdot \left(\left(\mu + \frac{\mu_T}{\sigma_k} \right) \nabla k \right) + P_k - \rho \varepsilon \quad (7)$$

where the production term is expressed as:

$$P_k = \mu_T \left(\nabla \mathbf{u} \times \left(\nabla \mathbf{u} + (\nabla \mathbf{u})^T \right) - \frac{2}{3} (\nabla \cdot \mathbf{u})^2 \right) - \frac{2}{3} \rho k \nabla \cdot \mathbf{u} \quad (8)$$

The transport equation for the turbulent dissipation rate is:

$$\rho \frac{\partial \varepsilon}{\partial t} + \rho \mathbf{u} \cdot \nabla \varepsilon = \nabla \cdot \left(\left(\mu + \frac{\mu_T}{\sigma_\varepsilon} \right) \nabla \varepsilon \right) + C_{\varepsilon 1} \frac{\varepsilon}{k} P_k - C_{\varepsilon 2} \rho \frac{\varepsilon^2}{k} \quad (9)$$

Table 1 Values of the constants in the turbulent model

Constant	Value
C_μ	0.09
$C_{\varepsilon 1}$	1.44
$C_{\varepsilon 2}$	1.92
σ_k	1.0
σ_ε	1.3

Values of the model constants in Eqs. (6), (7), and (9) are listed in Table 1.

3 Simulation and experimental study of the flow field in ED-milling

3.1 Overall flow field distribution analysis

Simulation software COMSOL was employed to simulate the flow field between the electrode and workpiece. In the simulation model, the inlet pressure of the working medium was set to 1.5 MPa, and the outlet pressure was set to 0.1 MPa. The electrode diameter was set to 20 mm. The central tube diameter was set to 6 mm, and the single-layer cutting thickness was set to 2 mm. The global and cross-sectional (along the X direction) flow velocities and pressure distributions of the working medium are shown in Fig. 3.

The flow velocity decreases with increasing distance to the inlet. When the working medium flows into the gap between the electrode and workpiece through the central inlet, the highest velocity occurs on the workpiece surface near the inner wall of the electrode. The velocity of the working medium flowing from outlet 1 is 22.57 m/s. The highest pressure occurs at the center of the inlet tube, and the pressure of the working medium decreases along the radial direction from the center of the electrode. The flow velocity and pressure in the discharge semicircular area between the electrode and workpiece are relatively low.

The volume proportions of the working medium flowing out of the discharge gap from outlets 1, 2, and 3 are shown in Fig. 4. It is observed that most of the working medium flows from outlet 3. This part of the working medium does not flow through the discharge area, and it does not contribute to the removal of discharge eroded particles from the discharge gap. Only the working medium flowing from outlets 1 and 2 could facilitate the eroded particle removal process, which accounts for 53.88% of the total inlet working medium. The volume ratio of the working medium flowing from outlets 1 and 2 is approximately 4:1, which indicates that more eroded particles are removed from the discharge gap through outlet 1.

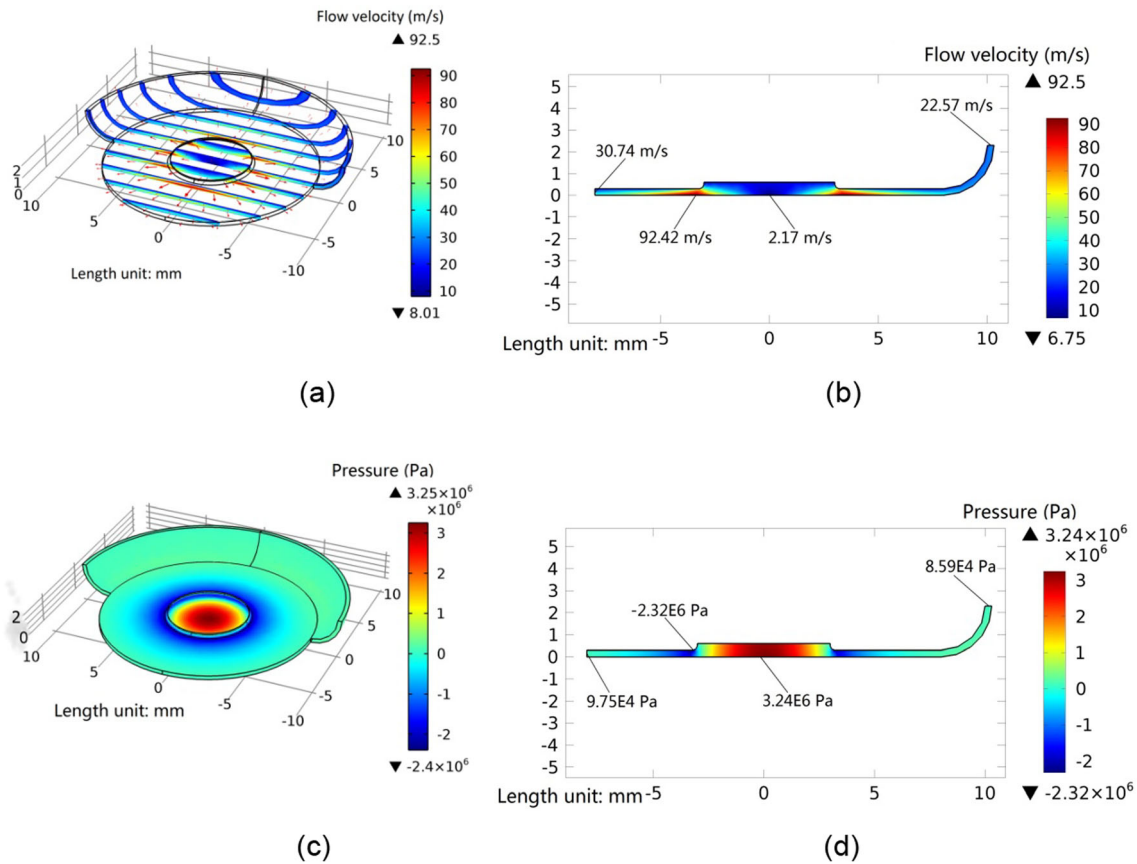


Fig. 3 Flow field of ED-milling with a tubular electrode. **a** Velocity distribution of the flow field. **b** Cross-sectional velocity distribution of the flow field. **c** Pressure distribution of the flow field. **d** Cross-sectional view pressure distribution of the flow field

3.2 The influence of the single-layer cutting thickness on the flow field and machining performance

When setting the diameter of the electrode to 20 mm and the flow pressure of the inlet working medium to 1.5 MPa, the influence of the single-layer cutting thickness on the flow field and machining performance is shown in Fig. 5. With increasing single-layer cutting thickness, the working medium volume flowing from outlets 2 and 3 increased, and the flow from

outlet 1 decreased. Moreover, with increasing single-layer cutting thickness, the proportion of the total working medium volume flowing from outlets 1 and 2, which effectively removes eroded particles from the gap, to the total inlet volume was lower than 50% when single-cutting layer thickness larger than 2 mm. This can be explained by the growing radius of the round chamfer at the bottom of the electrode due to the wearing process, which inhibits the flow of the working medium from the discharge gap through outlet 1, and more working medium flows from outlet 3 without passing through the discharge area.

The influence of the single-layer cutting thickness on the machining performance was experimentally studied based on the process parameters listed in Table 2. The MRR and TWR were calculated with Eqs. (10) and (11), respectively. As shown in Fig. 5b, with increasing single-layer cutting thickness, the MRR increased and the TWR decreased. The working medium flowing through the discharge area decreased with increasing single-layer cutting thickness, which led to some of the eroded particles not being removed from the gap and resolidifying on the workpiece surface. The tool electrode material is graphite, and its wearing process involves high-temperature

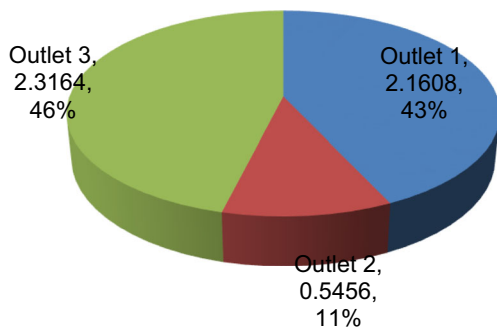
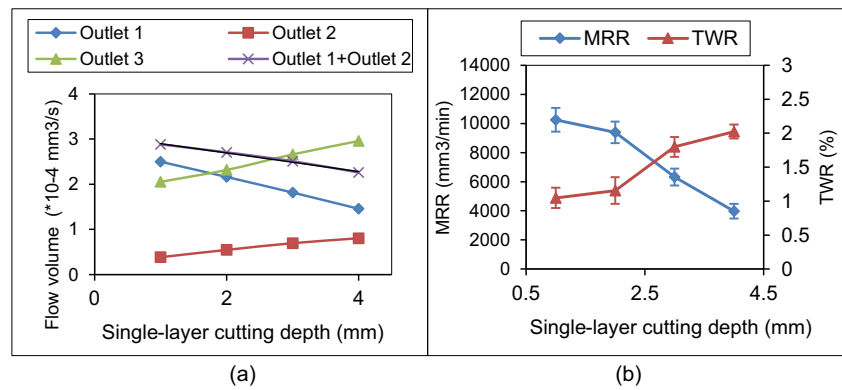


Fig. 4 Distribution of the working medium flowing from the different outlets

Fig. 5 Influence of the single-layer cutting thickness on the flow volume and machining performance. **a** Simulation results of the flow field. **b** Machining performance



sublimation. The reduction in the cooling effect owing to the increase in the single-layer cutting thickness leads to electrode wear increase.

$$MRR = \frac{l \cdot w \cdot d}{t} \quad (10)$$

where l (mm) is the length of the machined groove, w (mm) is the width of the machined groove, d (mm) is the depth of the machined groove, and t (s) is the machining time.

$$TWR = \frac{\Delta V_{\text{electrode}}}{\Delta V_{\text{workpiece}}} \quad (11)$$

where $\Delta V_{\text{electrode}}$ is the volume of the machined groove and $\Delta V_{\text{workpiece}}$ is the volume of the machined groove.

3.3 The influence of the electrode diameter on the flow field and machining performance

When the single-layer cutting thickness is 2 mm and the inlet flushing pressure is 1.5 MPa, the influence of the electrode diameter on the flow field and machining performance is shown in Fig. 6. With increasing electrode diameter, the volume of the working medium flowing from outlet 2 decreased and that flowing from outlet 3 increased. The change in

electrode diameter did not affect the volume of the working medium flowing from outlet 1. With increasing electrode diameter, the volume proportion of the working medium flowing from outlets 1 and 2 decreased, and it decreased to less than 50% when the electrode diameter was increased to 30 mm.

By setting the single-cutting layer thickness to 2 mm and adopting the same process parameters, as listed in Table 2, the influence of the electrode diameter on the machining performance was experimentally studied. The result is shown in Fig. 6b. The highest MRR was realized when using an electrode with a diameter of 20 mm. When the electrode diameter is small, the eroded particles are concentrated in a limited area, which makes them difficult to remove from the discharge gap. When the electrode diameter is large, the drop in the effective flushing working medium leads to a decrease in the MRR. The TWR decreased with increasing electrode diameter owing to the improvement in electrode heat conduction.

4 Improvement of the flow field in ED-milling

4.1 Improvement of the electrode structure

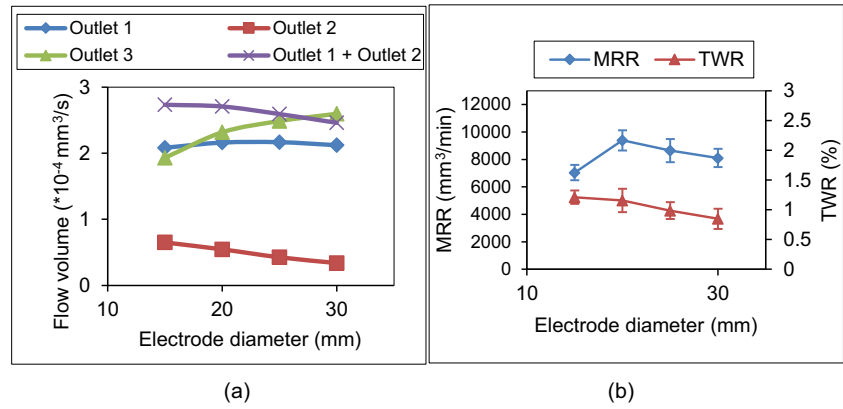
When the tool electrode with only a central hole was adopted, the working medium flowing through the discharge area was limited. To improve the flushing effect in the discharge gap, 3 types of electrodes with novel structures were designed, as summarized in Table 3. In regard to electrode 2, 12 holes with a diameter of 2 mm were designed around the central hole. In regard to electrode 3, the central hole was removed based on electrode 2. In regard to electrode 4, 20 holes with a diameter of 2 mm were designed along the outer wall of electrode 1.

Adopting the same volume of the inlet working medium, flow velocity simulation results for the 3 newly designed electrodes are shown in Fig. 7. As shown in Fig. 7a, when using electrode 2 as the tool electrode, the maximum flow velocity in the flow field decreased, but the flow velocity of the working medium flowing through the discharge area was enhanced. When using electrode 3 as the tool electrode, the

Table 2 Process parameters for the single-layer cutting thickness tests

Process parameters	Setting
Electrode material	Graphite
Workpiece material	Ti-6Al-4V
Working medium	Water-based emulsion
Pulse-on time (μ s)	2000
Pulse-off time (μ s)	100
Discharge current (A)	300
Electrode diameter (mm)	Outer, 20; inner, 6
Flushing pressure (MPa)	1.5
Electrode rotation speed (rpm)	600

Fig. 6 Influence of the electrode diameter on the flow volume and machining performance. **a** Simulation results of the flow field. **b** Machining performance



improvement of the flow field in the discharge area was limited over that depicted in Fig. 7a.

The simulation result for electrode 4 is shown in Fig. 7c. With 20 holes along the electrode outer wall, the working medium flowing from these holes directly flushes the discharge area. The main advantage of this electrode is its ability to flush the discharge area when the electrode starts the machining process from the outside of the workpiece. In this

case, the working medium flows through the discharge area and removes eroded particles from the discharge gap.

4.2 Comparison of the flushing effects of the different electrodes

Based on calculated flow fields for the above 4 kinds of electrode structures, a comparison of the volume and mean flow velocity of the working medium flowing from the different outlets is shown in Fig. 8. No obvious difference was found for the different electrodes.

In the ED-milling process, discharge mainly occurs on the front semicircular surface along the electrode feeding direction. The working medium flushing effect in this area plays a vital role in the eroded particle removal process. The flow velocity distribution on the front semicircular surface for the above 4 kinds of electrodes is shown in Fig. 9. It is observed that the different electrode structures result in obvious differences in the flow velocity distribution.

As shown in Fig. 9a, in regard to electrode 1 with only one central hole, the lowest flow velocity of the working medium occurred when the working medium was about to reach the upper surface of outlet 1. The lowest flow velocity was distributed in a ring shape, which prevented the working medium flow field in this area from being improved via electrode rotation. The low flow velocity in this area caused high-temperature eroded particles to easily readhere to the workpiece surface when the working medium flowed through this area.

As shown in Fig. 9b, in regard to electrode 2 with multiple holes around the central hole, the location of the lowest flow velocity occurred in the same area as that for electrode 1. However, the low-flow velocity area exhibited an intermittent pattern. When electrode rotation was adopted, the flow velocity in the low-velocity ring-shaped area intermittently increased and decreased, which was helpful to remove eroded particles from the discharge gap.

As shown in Fig. 9c, in regard to electrode 3 with only multiple holes distributed along the edge of the electrode, the location of the lowest flow velocity occurred in the same

Table 3 Details of the electrode structure

Model	Details	Structure
Electrode 1	Outer diameter: 20 mm; inner diameter: 6 mm	
Electrode 2	Outer diameter: 20 mm; inner diameter: 6 mm; diameter of surrounding 12 holes: 2 mm	
Electrode 3	Outer diameter: 20 mm; diameter of surrounding 12 holes: 2 mm	
Electrode 4	Outer diameter: 26, 20 mm; inner diameter: 6 mm; diameter of surrounding 20 holes: 2 mm;	

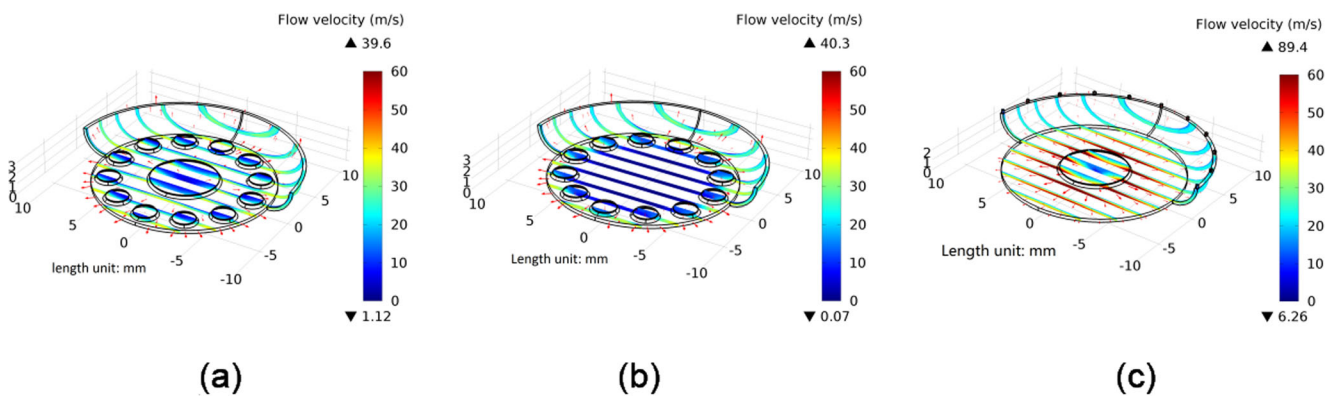


Fig. 7 Flow field using the electrode with the newly designed structure, a Electrode 2. b Electrode 3. c Electrode 4

Fig. 8 Flow field comparison for the different electrodes. a Flow volume. b Flow velocity

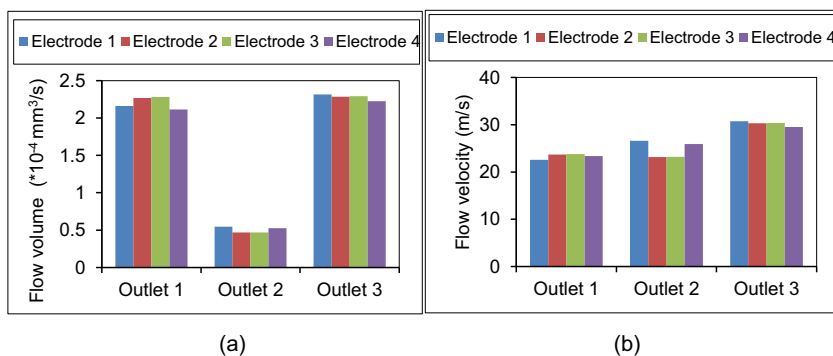


Fig. 9 Flow velocity distribution in the discharge area for the different electrodes. a Electrode 1. b Electrode 2. c Electrode 3. d Electrode 4

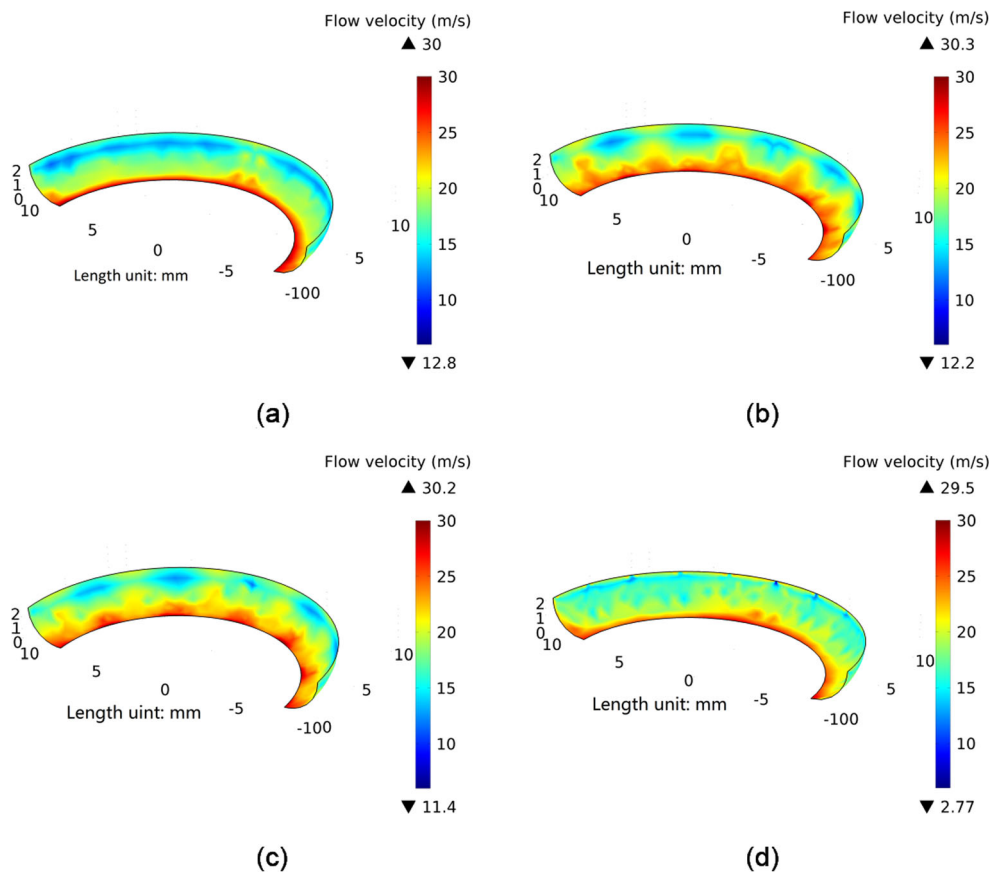


Table 4 Process parameters for the flushing effect comparison

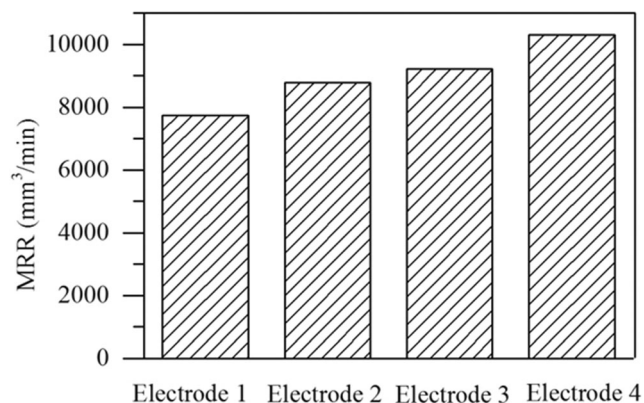
Process parameters	Setting
Electrode material	Graphite
Workpiece material	Ti-6Al-4V
Working medium	Water-based emulsion
Pulse-on time (μs)	2000
Pulse-off time (μs)	100
Discharge current (A)	400
Single-layer cutting thickness (mm)	2
Workpiece polarity	Positive
Flushing pressure (MPa)	1.5
Electrode rotation speed (rpm)	600

area as that for electrode 2, but the lowest-flow velocity area was further reduced.

As shown in Fig. 9d, in regard to electrode 4 with multiple holes surrounding the electrode outer wall, no significant low-velocity ring-shaped area was observed on the semicircular surface. This kind of flushing method was more conducive to the removal process of eroded particles.

4.3 The influence of the different electrodes on the machining efficiency

To study the machining performance of ED-milling for the four different electrode structures, a machining experiment was conducted using the process parameters listed in Table 4. The MRR result is shown in Fig. 10. The MRR was improved by the designed new electrode structure. When applying electrode 4 as the tool electrode, the MRR was 33% higher than that when applying electrode 1. This demonstrated that the flow field formed by electrode 4 facilitated the eroded particle removal process.

**Fig. 10** MRR comparison for the different electrodes

5 Conclusions

1. In regard to the tool electrode with only a central outlet hole, nearly half of the working medium flows out of the discharge gap along the direction opposite to the feeding direction, which does not flush the discharge area nor remove discharge eroded particles from the discharge gap.
2. Increasing the single-layer cutting thickness results in a decreased volume of the effective flushing working medium, which is not conducive to the removal process of eroded particles.
3. The diameter of the electrode influences the working medium flow field. For fixed process parameters, the optimal electrode diameter is experimentally found to yield the highest MMR.
4. The occurrence of a ring-shaped area with a low flow velocity on the front semicircular surface is the main problem for electrodes with only central hole. By designing 20 holes with a diameter of 2 mm surrounding the electrode outer wall, the flow field in the ring-shaped area is improved, and the MRR increases 33%.

Code availability Not applicable.

Funding This research is supported by the Fundamental Research Funds for the Central Universities of China (grant no. 2572017BB06).

Data availability The authors confirm that the data supporting the findings of this study are available within the article.

Declarations

Conflict of interest The authors declare no competing interests.

References

1. Ho KH, Newman ST (2003) State of the art electrical discharge machining (EDM). *Int J Mach Tool Manu* 43(13):1287–1300. [https://doi.org/10.1016/s0890-6955\(03\)00162-7](https://doi.org/10.1016/s0890-6955(03)00162-7)
2. Muthuramalingam T, Mohan B (2015) A review on influence of electrical process parameters in EDM process. *Arch Civil Mech Eng* 15(1):87–94. <https://doi.org/10.1016/j.acme.2014.02.009>
3. Ho KH, Newman ST, Rahimifard S, Allen RD (2004) State of the art in wire electrical discharge machining (WEDM). *Int J Mach Tool Manu* 44(12-13):1247–1259. <https://doi.org/10.1016/j.ijmachtools.2004.04.017>
4. Fujimoto T, Okada A, Okamoto Y, Uno Y (2012) Optimization of nozzle flushing method for smooth debris exclusion in wire EDM. *Key Eng Mater* 516:73–78. <https://doi.org/10.4028/www.scientific.net/KEM.516.73>
5. Wang F, Liu Y, Zhang Y, Tang Z, Ji R, Zheng C (2014) Compound machining of titanium alloy by super high speed EDM milling and arc machining. *J Mater Process Technol* 214(3):531–538. <https://doi.org/10.1016/j.jmatprotec.2013.10.015>
6. Pillai KVA, Hariharan P, Jafferson JM (2019) μ ED milling of Ti-6Al-4V using cryogenic-treated Wc tool and nano-graphene

- powder-mixed dielectric different discharge energy regimes. *Int J Adv Manuf Technol* 102(9-12):2721–2743. <https://doi.org/10.1007/s00170-019-03327-8>
7. Zhou T, Zhou C, Liang Z, Wang X (2017) Machining mechanism in tilt electrical discharge milling for lens mold. *Int J Adv Manuf Technol* 95(5-8):2747–2755. <https://doi.org/10.1007/s00170-017-1408-5>
 8. Chakraborty S, Dey V, Ghosh SK (2015) A review on the use of dielectric fluids and their effects in electrical discharge machining characteristics. *Precis Eng* 40:1–6. <https://doi.org/10.1016/j.precisioneng.2014.11.003>
 9. Shen Y, Liu Y, Sun W (2016) High-efficient dry hybrid machining of EDM and arc machining. *Procedia CIRP* 42:149–154. <https://doi.org/10.1016/j.procir.2016.02.210>
 10. Liu Y, Chang H, Zhang W, Ma F, Sha Z, Zhang S (2018) A Simulation study of debris removal process in ultrasonic vibration assisted electrical discharge machining (EDM) of deep holes (dagger). *Micromachines* 9(8). <https://doi.org/10.3390/mi9080378>
 11. Mullya S, Karthikeyan G, Ganachari V (2020) An investigation into performance of electric discharge milling using slotted tools. *J Mech Sci Technol* 34(6):2525–2533. <https://doi.org/10.1007/s12206-020-0528-2>
 12. Wang X, Shen Y (2019) High-speed EDM milling with in-gas and outside-liquid electrode flushing techniques. *Int J Adv Manuf Technol* 104(5-8):3191–3198. <https://doi.org/10.1007/s00170-019-04242-8>
 13. Okada A, Uno Y, Onoda S, Habib S (2009) Computational fluid dynamics analysis of working fluid flow and debris movement in wire EDMed kerf. *CIRP Ann* 58(1):209–212. <https://doi.org/10.1016/j.cirp.2009.03.003>
 14. Wang J, Han F (2014) Simulation model of debris and bubble movement in electrode jump of electrical discharge machining. *Int J Adv Manuf Technol* 74(5-8):591–598. <https://doi.org/10.1007/s00170-014-6008-z>
 15. Chang WJ, Xi YY, Li HW (2020) Simulation of gap flow field in EDM process used oil-in-water working fluid. *Key Eng Mater* 841: 232–237. <https://doi.org/10.4028/www.scientific.net/KEM.841.232>
 16. Feng G, Yang X, Chi G (2018) Experimental and simulation study on micro hole machining in EDM with high-speed tool electrode rotation. *Int J Adv Manuf Technol* 101(1-4):367–375. <https://doi.org/10.1007/s00170-018-2917-6>
 17. Wang YQ, Bai JC, Guo YF, Huang H (2011) Investigation of the effects of dielectric inlet pressure in inner jetted dielectric EDM milling. *Adv Mater Res* 189-193:125–128. <https://doi.org/10.4028/www.scientific.net/AMR.189-193.125>
 18. Shabgard M, Ahmadi R, Seyedzavvar M, Oliaei SNB (2013) Mathematical and numerical modeling of the effect of input-parameters on the flushing efficiency of plasma channel in EDM process. *Int J Mach Tool Manu* 65:79–87. <https://doi.org/10.1016/j.ijmachtools.2012.10.004>
 19. Liao YS, Wu PS, Liang FY (2013) Study of debris exclusion effect in linear motor equipped die-sinking EDM process. *Procedia CIRP* 6:123–128. <https://doi.org/10.1016/j.procir.2013.03.058>
 20. Wang Z, Tong H, Li Y, Li C (2018) Dielectric flushing optimization of fast hole EDM drilling based on debris status analysis. *Int J Adv Manuf Technol* 97(5-8):2409–2417. <https://doi.org/10.1007/s00170-018-2141-4>
 21. Kunieda M, Kitamura T (2018) Observation of difference of EDM gap phenomena in water and oil using transparent electrode. *Procedia CIRP* 68:342–346. <https://doi.org/10.1016/j.procir.2017.12.065>

Publisher's note Springer Nature remains neutral with regard to jurisdictional claims in published maps and institutional affiliations.